Long-term, in vivo therapeutic effects of a single dose of miR-145 micelles for atherosclerosis

Deborah D. Chin [a], Neil Patel [a], Woori Lee [a], Sonali Kanaya [a], Jackson Cook [a], Eun Ji Chung [a,b,c,d,e,f,*]

[a] Department of Biomedical Engineering, University of Southern California, Los Angeles, CA, 90089, United States
[b] Division of Vascular Surgery and Endovascular Therapy, Department of Surgery, Keck School of Medicine, University of Southern California, Los Angeles, CA, 90033, United States
[c] Mork Family Department of Chemical Engineering and Materials Science, University of Southern California, Los Angeles, CA, 90089, United States
[d] Eli and Edythe Broad Center for Regenerative Medicine and Stem Cell Research, Keck School of Medicine, University of Southern California, Los Angeles, CA, 90033, United States
[e] Division of Nephrology and Hypertension, Department of Medicine, Keck School of Medicine, University of Southern California, Los Angeles, CA, 90033, United States
[f] Norris Comprehensive Cancer Center, Keck School of Medicine, University of Southern California, Los Angeles, CA, 90089, United States

A R T I C L E   I N F O

A B S T R A C T

Atherosclerosis is a chronic inflammatory disease that is characterized by the build-up of lipid-rich plaques in the arterial walls. The standard treatment for patients with atherosclerosis is statin therapy aimed to lower serum lipid levels. Despite its widespread use, many patients taking statins continue to experience acute events. Thus, to develop improved and alternative therapies, we previously reported on microRNA-145 (miR-145 micelles) and its ability to inhibit atherosclerosis by targeting vascular smooth muscle cells (VSMCs). Importantly, one dose of miR-145 micelles significantly abrogated disease progression when evaluated two weeks post-administration. Thus, in this study, to evaluate how long the sustained effects of miR-145 micelles can be maintained and towards identifying a dosing regimen that is practical for patients with chronic disease, the therapeutic effects of a single dose of miR-145 micelles were evaluated for up to two months in vivo. After one and two months post-treatment, miR-145 micelles were found to reduce plaque size and overall lesion area compared to all other controls including statins without causing adverse effects. Furthermore, a single dose of miR-145 micelle treatment inhibited VSMC transdifferentiation into pathogenic macrophage-like and osteogenic cells in plaques. Together, our data shows the long-term efficacy and sustained effects of miR-145 micelles that is amenable using a dosing frequency relevant to chronic disease patients.

1. Introduction

Atherosclerosis causes death in 1 in 4 people and is a chronic inflammatory disease in which calcified, lipid-rich lesions within the vessel wall can abruptly rupture leading to sudden death [1,2]. Since the 1980's, drug interventions to slow atherosclerosis progression have focused primarily on lowering plasma cholesterol levels by inhibiting cholesterol synthesis using statins. Despite its wide distribution, statins do not benefit all patients [3–8]. After 5 years of statin therapy, there is only ~20% reduction of myocardial infarction or stroke incidence, and ~80% of the 35 million patients in the US that take a statin will have a

secondary event [9–12]. Other drugs such as ezetimibe are also available to lower blood cholesterol levels by blocking small intestine cholesterol absorption, thus, freeing up liver cells to remove low density lipoprotein (LDL) cholesterol directly from blood. However, the effects of ezetimibe are modest, reducing cardiovascular risk by only 2% and are only prescribed in combination with statins to patients with high LDL cholesterol levels [13]. Therefore, there is a significant need for developing new therapeutic targets and strategies beyond lipid lowering for atherosclerosis.

Recently, vascular smooth muscle cells (VSMCs) residing within the medial layer of the vascular wall have become recognized for their
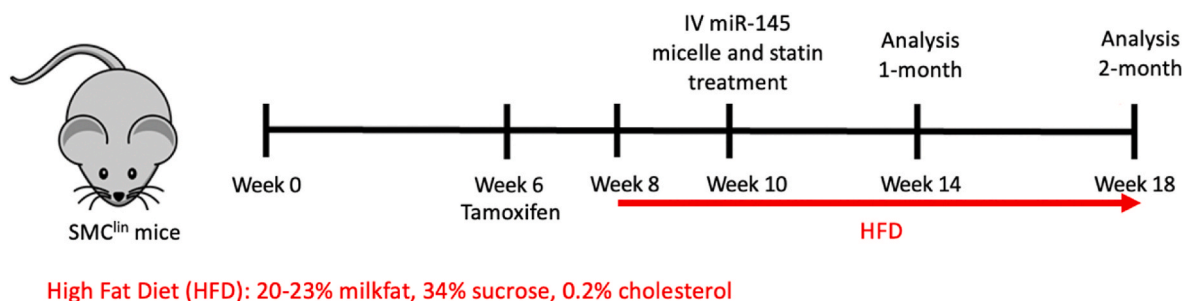
Fig. 1. Timeline of SMC^{lin} model with high fat diet and treatment for one-month and two-months endpoints.

integral role in the progression of atherosclerosis and represent a novel target for atherosclerosis treatment [14]. In early atherosclerosis, quiescent, contractile VSMCs dedifferentiate into a synthetic phenotype and overproliferate and migrate into the intima [15,16]. Upon disease progression, VSMCs transdifferentiate into alternative phenotypes that resemble macrophages, foam cells, and osteochondrogenic cells [14, 17–20]. Inflammatory, macrophage-like cells and foam cells form the necrotic core and osteochondrogenic-like cells form calcifications that destabilize the plaque and increase their susceptibility for rupture [21–24]. However, despite transformation into atherogenic cell types, VSMCs retain remarkable plasticity that enable them to revert back into the healthy, contractile state [15,16,25]. Thus, this critical transition can be used to develop VSMC-targeted, atherosclerosis therapies.

Previously, we reported on the efficacy of microRNA-145 (miR-145) as a therapy for atherosclerosis when delivered as part of a targeted, drug delivery system using micelle nanoparticles [26,27]. MicroRNAs are short, non-coding RNAs that regulate gene expression post-transcriptionally via complementary base pair matching with mRNA, and specifically, miR-145 is a key regulator in promoting contractile VSMCs by binding to and inhibiting Krüppel-like factor-4 (KLF4) and ETS like-1 protein (ELK1) which promote VSMC dedifferentiation into pathogenic phenotypes [25,28,29]. To incorporate miR-145 into micelles, we covalently conjugated miR-145 to 1, 2-distearoyl-sn-glycer-o-3-phosphoethanolamine-poly (ethylene glycol)2000 (DSPE-PEG (2000)) to create miR amphiphiles. Then, miR-145 amphiphiles were mixed with amphiphiles containing peptides that bind to C–C chemokine receptor-2 (CCR2) expressed on synthetic VSMCs to form VSMC-targeting, miR-145 micelles [30,31]. In vivo, we verified that miR-145 micelles treatment resulted in a 43% reduction in plaque size compared to non-treated controls when administered throughout disease progression in the advanced atherosclerotic mouse model [26]. Importantly and surprisingly, early-stage atherosclerotic mice treated with only a single dose of miR-145 micelles also showed remarkable efficacy with a 49% reduction in plaque growth compared to no treatment and a 54% reduction compared to free miRs when assessed two weeks after treatment.

Currently, there are 16 FDA approved RNA therapies using subcutaneous and intravenous administration and dosing regimens ranging from injections biweekly to biannually [32–34]. Particularly for chronic diseases such as atherosclerosis, ideal RNA-based therapies should have long-lasting effects that require fewer dosages while still maintaining a therapeutic response. Thus, a critical step towards translation of miR-145 micelles into the clinic is to evaluate the longer-term effects and a practical dosing regimen for patients with chronic disease.

To that end, in the present study, we investigate the prolonged therapeutic effects of miR-145 micelles for atherosclerosis after one dose for up to two months post-administration in the *Myh11*-CreER^{T2} ROSA*26* STOP-flox eYFP$^{+/+}$ *Apoe*$^{-/-}$ mice (SMC^{lin} mice) that enables tracking VSMC-derived cells throughout atherosclerosis progression. We analyzed the size and extent of lesion formation in the aorta, evaluated the composition of VSMC-derived cell types within plaques, and assess the safety or miR-145 micelles. Our studies aim to evaluate the viability

of miR-145 micelles as an alternative therapy to current standard of care medications and to determine a micelle dosing frequency that is amenable to chronic disease patients towards an effort for their eventual implementation in the clinic.

2. Experimental

Synthesis of amphiphiles. MCP-1 and scrambled peptides were synthesized using standard Fmoc solid-phase peptide synthesis procedures previously published [26,30,35–37]. MCP-1 peptide (0.25 mmol) [YNFTNRKISVQRLASYRRITSSK] or scrambled (NT) peptide (0.25 mmol) [YNSLVFRIRNSTQRKYRASIST] were synthesized on an automated peptide synthesizer (PS3, Protein Technologies, Tucson, AZ) using Wang resin. The peptides were cleaved from the resin using a solution of 94:2:5:2.5:1 vol% trifluoroacetic acid:1,2-ethanedithiol: water:triisopropylsilane over a 4 h reaction. Peptides were precipitated, washed twice with ice-cold diethyl ether, lyophilized, and stored at −20 °C until purification via reverse-phase high performance liquid chromatography system (HPLC, Prominence, Shimadzu, Columbia, MD). Purified peptides were conjugated to DSPE-PEG (2000)-maleimide to synthesize peptide amphiphiles. Synthesis reactions occurred in pH 7.4 buffered water before purification via HPLC. Expected m/z peaks were verified using MALDI-TOF at $[M+H]^+ = 5830$.

miR-145 (5′-GUCCAGUUUUCCCAGGAAUCCCU-3′) and control miR (miR-67) (5′-UCACAACCUCCUAGAAAGAGUAGA-3′) were ordered from IDT (Coralville, IA) with a thiol modified 5′ end of the sense (functional) strand to covalently conjugate the microRNA to the lipid tail. miR-145-SH (MW = 14,490 g/mol) was treated with TCEP and stirred in the dark at room temperature for 4 h at 1600 rpm. Thiolated miR-145 was conjugated to DSPE-PEG (2000)-maleimide (Avanti Polar Lipids, Alabaster, AL) via a thioether bond by adding a 10% molar excess of lipid to reduced thiolated miR in DEPC-treated water. The resulting products were characterized using MALDI.

VSMC transdifferentiation in vitro. Mouse aortic smooth muscle cells (ATCC) were cultured in DMEM supplemented with 10% FBS to 60–70% confluency followed by treatment with either 250 nM miR-145 micelles or PBS for 12 h. Following treatment, cells were either incubated with 10 μg/mL methyl-β-cyclodextrin cholesterol (MBD-Chol; Millipore Sigma) for 3 days to induce macrophage differentiation or 2.5 mM Na$_2$HPO$_4$ and 2.7 mM CaCl$_2$ for 5 days to induce osteoblast differentiation [38,39]. Cells were then immunostained. Briefly, cells were fixed in 4% paraformaldehyde and permeabilized with 0.05% Tween-20. Cells were washed in PBS, incubated for 30 min with mouse FCR blocking solution (Miltenyi), and then incubated overnight at 4 °C with either Alexa Fluoro-488 conjugated anti-CD68 antibody (1:200, Thermofisher 25747-1-AP) or PE-conjugated anti-RUNX2 antibody (1:200, CellSignaling 98059S) in blocking solution. Cells were then washed in PBS and analyzed by flow cytometry on a Attune NXT cytometer (Thermofisher) with 488 nm and 561 nm laser lines, gating to remove cell debris, aggregates, and maintaining singlets.

Mice. Animal protocols were approved by the University of Southern California Institutional Animal Care and Use Committee (IACUC). Male

Myh11-CreER^{T2} ROSA26 STOP-flox eYFP$^{+/+}$ *Apoe$^{-/-}$* mice and female *Apoe$^{-/-}$* mice. Male littermate controls were used for all studies as the *Myh11* transgene is expressed only in male mice. Mice were genotyped by qPCR. Following previously reported methods [28], mice received ten intraperitoneal injections of 1 mg tamoxifen from 6 weeks of age to 8 weeks for 10 mg total of tamoxifen per 25 g of mouse body weight to activate eYFP expression in MYH11 expressing SMCs.

Subsequently, mice were fed a high fat diet (20–23% milkfat, 34% sucrose, 0.2% cholesterol, Teklad Envigo) for 2 weeks before intravenous tail vein injection of treatment (miR-145 micelles, miR-67 micelles, scrambled MCP-1 (NT) miR-145 micelles, free miR-145 (1 mg/kg miR or 0.7 mM total micelle), or PBS). Mice in the statin treatment group were administered atorvastatin (Sigma Aldrich, St. Louis, MO) at a dose of 10 mg/kg in saline via oral gavage. Mice continued high fat diet for an additional 4 weeks or 8 weeks for short- and longer-term efficacy analyses (Fig. 1). Mice were then euthanized via CO$_2$ asphyxiation and perfused with PBS, 4% paraformaldehyde (PFA), and PBS again. Organs and aorta were carefully dissected and saved for additional analyses.

Analysis of atherosclerotic lesions. Atherosclerotic plaques were analyzed in two ways: 1) en face analysis of entire aorta with Oil Red O (ORO) lipid stain and 2) hematoxylin and eosin (H&E) stains of cross sections of aortic roots. Briefly, aortas were dissected from the root to the common iliac arteries. Excess adventitial fat was carefully removed and the aorta was fixed in 4% PFA overnight. The tissue was then cleaned in 78% methanol for 5 min before staining for 1 h with 0.2% ORO solution in methanol. The aortas were then washed twice with 78% methanol for 5 min each and cut open longitudinally before imaging with a stereomicroscope (Leica, Wetzlar, Germany). Quantification of positively stained lesions was done using ImageJ software (NIH, Bethesda, MD). Aortic roots were embedded in optimal cutting temperature compound (OCT) and flash frozen in 2-methylbutane and liquid nitrogen. Roots were sectioned at 10 μm thick sections and stained using H&E. Plaque and necrotic core area in three aortic root sections were quantified and averaged for each sample to obtain a mean ± S.D. measurement.

In vivo miR-145 expression. Aortic roots and liver tissue were obtained from treated mice. Tissues were weighed and lysed with Trizol (Invitrogen, Carlsbad, CA). miRNeasy Mini Kit (Qiagen, Hilden, Germany) was used to extract microRNA and the miScript II RT Kit (Qiagen, Hilden, Germany) was used to synthesize cDNA according to manufacturer's instructions. Real-time RT-qPCR was performed on the LightCycler 480 Real-Time PCR System (Bio-Rad Laboratories, Hercules, CA) to evaluate miR-145 levels. RNU-6 was used as an internal control and the 2-ΔΔCT method was used to calculate relative expression changes.

In vivo immunohistochemistry. Aortic roots were cryosectioned as mentioned above. Tissue sections were blocked in 10% donkey serum with 1% BSA. Sections were subsequently stained with antibodies to GFP (Abcam ab6673) to amplify YFP signal, α-SMA (Abcam ab5694), CD68 (Abcam ab125212), and RUNX2 (Abcam ab192256) overnight at 4 °C. Donkey anti-rabbit IgG Alexa Fluor 594 (Thermo Fisher, Waltham, MA, USA) and donkey anti-goat IgG Alex Fluor 488 (Thermo Fisher, Waltham, MA, USA) were used as secondary antibodies. Sections were counterstained with DAPI for the nuclei, mounted in ProLong Gold Antifade (Thermo Fisher, Waltham, MA, USA), and imaged using a confocal microscope (Nikon C2 CLSM, Nikon, Tokyo, Japan). Cells were then counted using ImageJ software. Current expression of alternative phenotype markers in VSMCs was compared with eYFP expression to determine transdifferentiation or retention of SMC phenotype.

Histological analysis of organs. Heart, lung, liver, spleen, intestine, and kidneys were removed from the euthanized mice. Organs were flash frozen in OCT and cryosectioned at 10 μm thick slices. Tissue sections were stained with H&E, imaged (Leica DMi8, Leica, Wetzlar, Germany), and tissue morphology was analyzed.

Cholesterol quantification. Serum cholesterol levels were quantified using a high-density lipoprotein (HDL) and low-density lipoprotein (LDL) quantification kit (Sigma-Aldrich). Following the manufacturer's protocol, HDL and LDL were separated in serum using precipitation buffer. HDL and LDL samples were subsequently incubated with Reaction Mixes and fluorescence (ex: 535 nm/em: 587 nm) was measured using a plate reader (Varioskan LUX, Thermo Fisher, Waltham, MA, USA).

Statistical analysis. Results are stated as means ± standard deviation (S.D.). Statistical analyses of the data were performed using a one-way analysis of variance (ANOVA) for more than two groups. A p value < 0.05 was considered statistically significant. All statistical analyses were performed using GraphPad Prism 8 (GraphPad Software, San Diego, CA).

3. Results and discussion

3.1. Single dose miR-145 micelle effects on atherosclerosis after one month

3.1.1. Therapeutic evaluation after one month

miR-145 micelles were synthesized by self-assembling miR-145 amphiphiles, MCP-1 amphiphiles, and DSPE-PEG (2000)-methoxy amphiphiles at a 1:49:50 mol ratio as previously described, to formulate a micelle nanoparticle with optimized particle charge, size, and therapeutic dose that enabled efficient cellular uptake, endosomal escape, and gene regulation [26,30]. Non-targeting miR-145 micelles (NT miR-145 micelles) and control miR-67 micelles were synthesized as previously described [26]. miR-145 micelle nanoparticles are approximately 21.7 nm with zeta potential of 15.1 mV, NT miR-145 micelles are approximately 23.3 nm with a zeta potential of 8.06 mV, and miR-67 micelles are 21.5 nm in size with a zeta potential of 11.8 mV [26].

We previously observed sustained miR-145 upregulation in aortic tissue two weeks after a single IV injection of miR-145 micelles in ApoE−/− mice despite an elimination half-life of 10.3 h [26], suggesting miR-145 micelles may have prolonged therapeutic effects beyond the initial circulation period, as also previous found for similar siRNA therapies [40,41]. For the treatment of chronic diseases such as atherosclerosis, long-term therapeutic effects of drugs are desirable as they lead to fewer dosages and enhanced patient compliance. To determine the optimal dosing interval of miR-145 micelles, we assessed the therapeutic effect and miR-145 upregulation one month after injection.

The primary mechanism of action for miR-145 micelles is through inhibition of VSMC transformation into pathogenic phenotypes such as macrophages that form the necrotic core and osteochondrogenic cells that produce plaque destabilizing calcifications [42,43]. We confirmed that miR-145 micelle treatment inhibits mouse aortic smooth muscle cell transdifferentiation into proatherogenic macrophage- and osteoblast-like phenotypes in vitro using flow cytometry (Supplemental Fig. 1). For in vivo analyses, the assessment of VSMC cell composition in plaques involves immunohistochemical analysis of vascular plaque tissue with conventional VSMC markers such as myocardin and Myosin Heavy Chain 11 (MYH11). However, as VSMCs dedifferentiate, they lose expression of these markers, making it difficult to assess the pathogenic cells in the plaque that have transformed from VSMCs, and subsequently, the effect of any therapy after disease development [44]. As such, for our studies, we utilized atherosclerotic SMC^{lin} mice due to the unique capability to identify VSMCs despite transdifferentiation. When SMC^{lin} mice are intraperitoneally administered tamoxifen, eYFP expression is activated in MYH11-expressing cells. Despite transdifferentiation, newly differentiated osteochondrogenic-like and macrophage-like cells of VSMC origin will continue to express eYFP, which enables tracing of pathogenic cells back to their SMC origin. Thus, this model allows for evaluating the effects of therapies like miR-145 micelles that target VSMCs throughout their evolution and throughout atherosclerosis disease progression [28,44].

Briefly, mice were given a high fat diet for two weeks to induce a state of developing atherosclerosis and treated with miR-145 micelles,
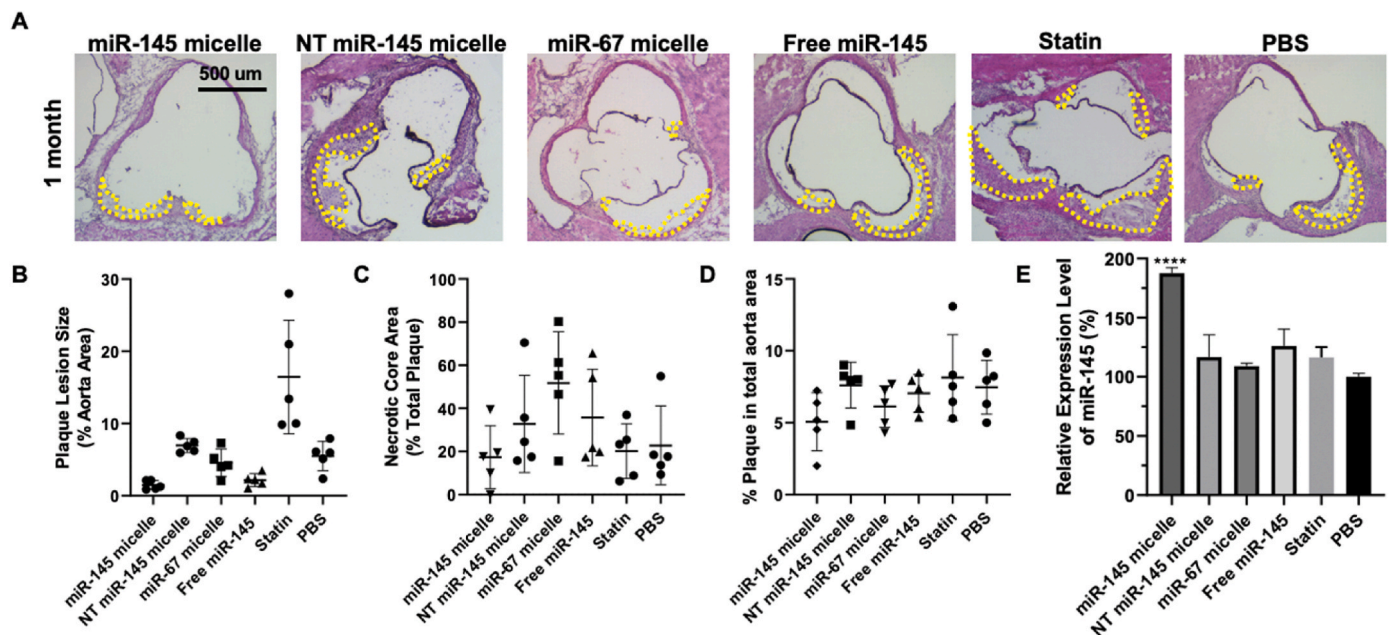
Fig. 2. Plaque analysis in early-stage atherosclerotic mice one month after treatment with a single dose of miR-145 micelles. (A) Cross sections of aortic roots of miR-145 micelle-treated mice stained with H&E. Yellow outlines indicate plaque area. Scale bar 500 μm. Quantification of (B) aortic root lesion sizes and (C) aortic root plaque necrotic core area, and (D) en face lesions of the aorta. (E) miR-145 expression in the aortic root quantified by RT-qPCR. ** indicates $p < 0.01$, **** indicates $p < 0.0001$.
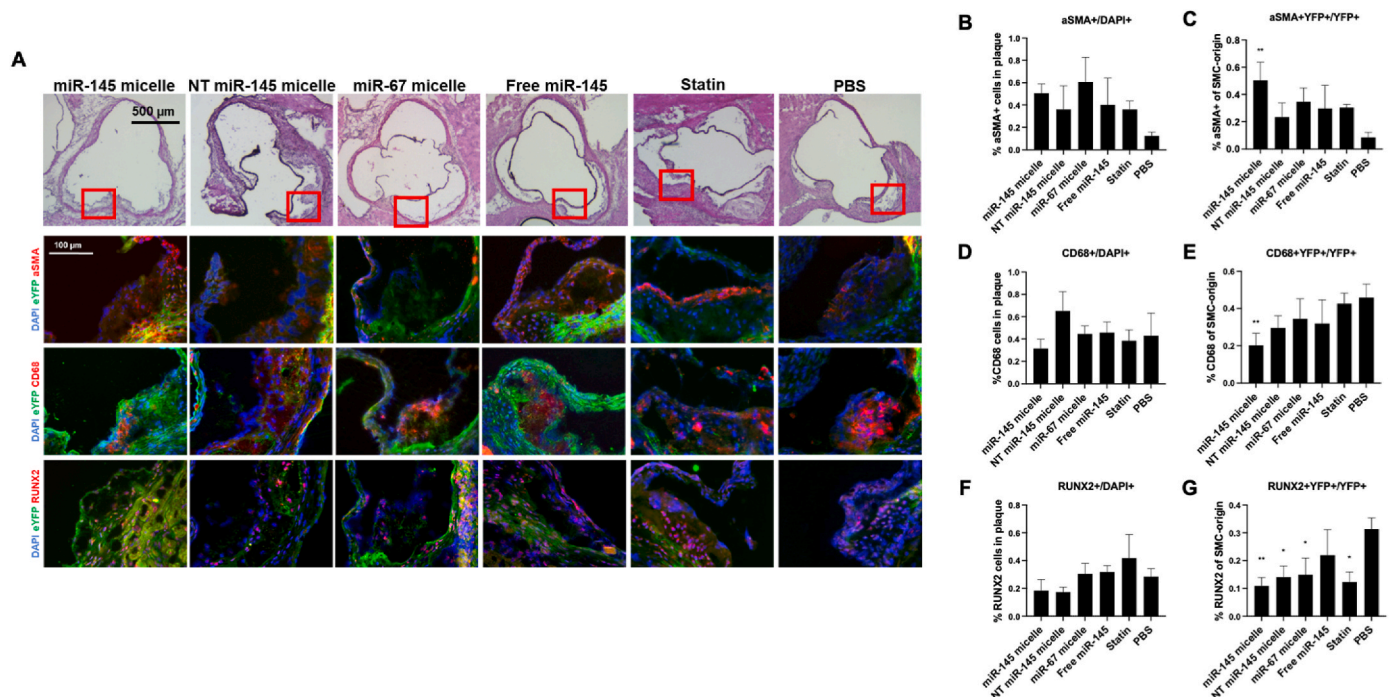

Fig. 3. Cellular composition of early-stage atherosclerotic plaque one month after treatment with a single dose of miR-145 micelles. (A) Immunohisto-chemistry of aortic root plaques for eYFP (green), α-SMA, CD68, RUNX2 (red), and nuclei (blue). Red boxes on H&E images indicate zoomed in areas of aortic root (bottom). Quantification of cells expressing (B) α-SMA+/DAPI, (C) α-SMA + YFP+/YFP+, (D) CD68+/DAPI, (E) CD68 + YFP+/YFP+, (F) RUNX2+/DAPI, and (G) RUNX2+YFP+/YFP+. VSMC marker expression with respect to YFP is used to analyze all VSMC-originating cells. * indicates $p < 0.05$, ** indicates $p < 0.01$.

non-targeting scrambled MCP-1 micelles with miR-145 (NT miR-145 micelles), MCP-1 micelles with non-therapeutic miR-67 (miR-67 mi-celles), free miR-145 at 1 mg/kg miR, atorvastatin (statin) at 3 mg/kg, or PBS [26]. After one-month after treatment, miR-145 micelle-treated mice were found to have the smallest plaque area within the aortic root compared to all other treatments (miR-145 micelle: 1.5 ± 0.6%, NT

miR-145 micelle: 7.0 ± 1.0%, miR-67 micelle: 4.6 ± 1.9%, free miR-145: 2.1 ± 0.9%, statin 16.4 ± 7.9%, PBS: 5.5 ± 2.0%, $p < 0.01$ for miR-145 micelle compared to PBS, Fig. 2A and B). However, the necrotic core area for the miR-145 micelle group at this time point was not significantly different compared to PBS treatment (Fig. 2C).

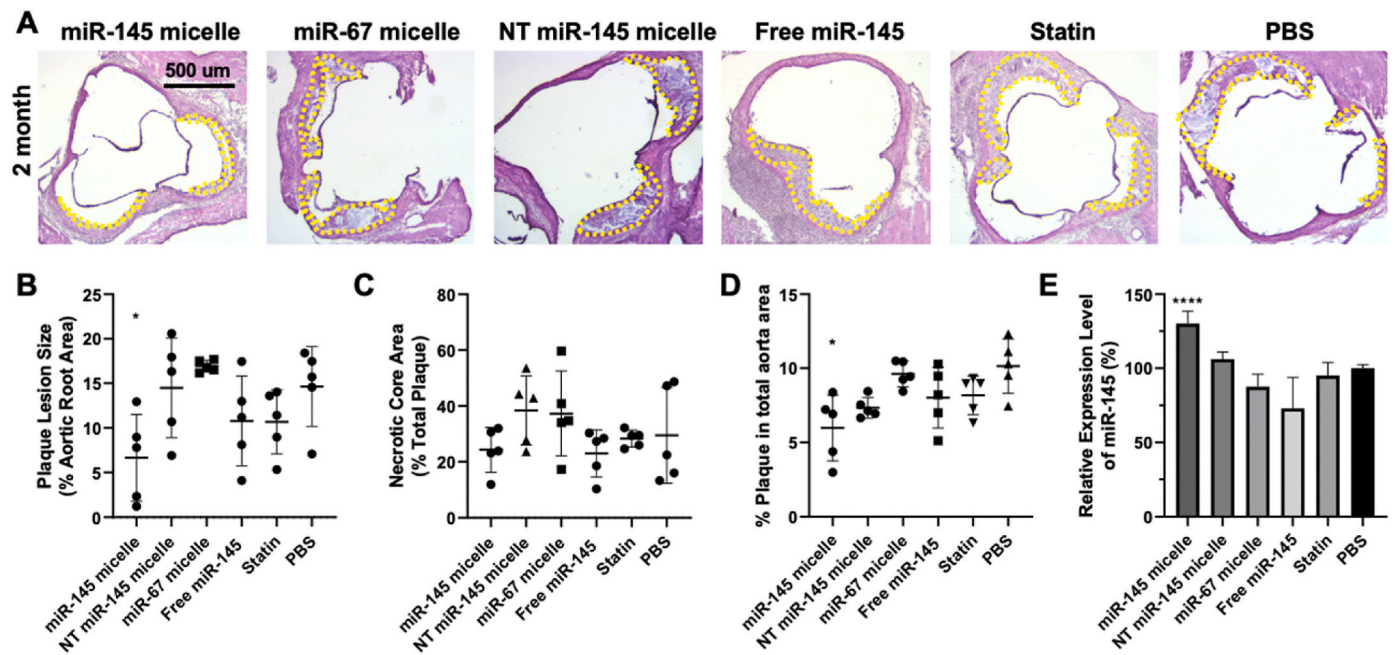Additionally, the overall lesion area of the aortas, from the aortic

Fig. 4. Plaque analysis in mid-stage atherosclerotic mice two months after treatment with a single dose of miR-145 micelles. (A) H&E stains of aortic root cross sections of miR-145 micelle-treated mice two months after treatment. Yellow dashes delineate plaque area. Quantification of (B) aortic root lesion sizes and (C) aortic root plaque necrotic core area, and (D) en face lesions in the entire aorta. (E) miR-145 expression in the aortic root is elevated with miR-145 micelle treatment when quantified by RT-qPCR. * indicates $p < 0.05$, **** indicates $p < 0.0001$.

root to the iliac arteries, were quantified using ORO en face staining. Although miR-145 micelle resulted in smaller total lesion area compared
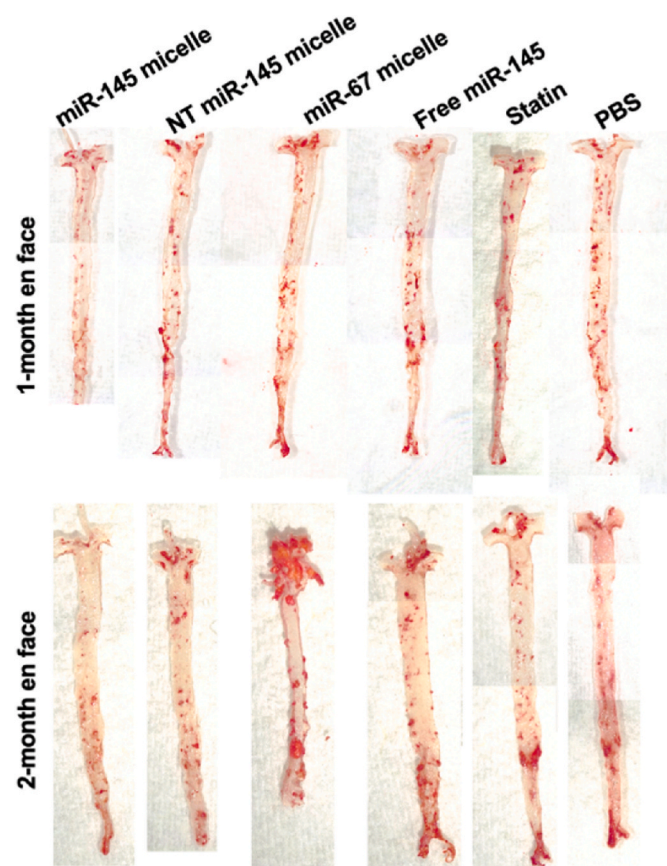

Fig. 5. ORO en face staining of the aorta after one- or two-months post-treatment of a single dose of miR-145 micelles.

to other treatments, no statistically significant differences were found at this time point (miR-145 micelle: $5.1 \pm 2.0\%$, NT miR-145 micelle: $7.6 \pm 1.6\%$, miR-67 micelle: $6.1 \pm 1.4\%$, free miR-145: $7.0 \pm 1.3\%$, statin: $8.1 \pm 3.0\%$, PBS: $7.5 \pm 1.0\%$, $p = 0.08$ for miR-145 micelles compared to PBS, Fig. 2D). Furthermore, miR-145 expression in the aortic root was analyzed via RT-qPCR. Notably, miR-145 micelle treatment sustained elevated levels of miR-145 expression in the aortic root by almost 1.8-fold ($p < 0.001$ compared to PBS and statin groups). This increase in miR-145 is comparable to the expression level at two weeks post-treatment from our previous studies which was also approximately 1.8-fold greater than non-treatment controls [26].

3.1.2. Cellular composition of atherosclerotic plaques after one month

To comprehensively investigate the effect of miR-145 micelle therapy on VSMC sub-phenotypes, aortic roots of treated SMC^{lin} mice were sectioned and stained for different VSMC phenotypes: α-smooth muscle actin (α-SMA, contractile VSMC), CD68 (macrophage-like cells), and RUNX2 (osteogenic cells, Fig. 3A). As shown in Fig. 3, PBS treatment resulted in the lowest α-SMA expression within plaques (miR-145 micelle: $50.6 \pm 8.4\%$, NT miR-145 micelle: $36.5 \pm 27.7\%$, miR-67 micelle: $60.3 \pm 30.5\%$, free miR-145: $40.1 \pm 30.7\%$, statin: $36.9 \pm 7.2\%$, PBS: $12.7 \pm 2.5\%$, Fig. 3B) demonstrating that the majority of VSMCs in the plaque have dedifferentiated from contractile VSMCs. In contrast, miR-145 micelle treatment showed the greatest overlap in eYFP and α-SMA signal ($50.3 \pm 13.3\%$, $p < 0.01$, Fig. 3C) compared to other treatments (NT miR-145 micelle: $23.3 \pm 14.4\%$, miR-67 micelle: $34.9 \pm 11.2\%$, free miR-145: $30.0 \pm 22.1\%$, statin: $30.7 \pm 2.5\%$, PBS: $9.3 \pm 2.7\%$), suggesting that miR-145 micelles preserve contractile VSMC phenotype and prevent the adoption of alternative phenotypes for up to a month after a single dose treatment [26].

Furthermore, overall percentages of CD68^{+} ($31.5 \pm 0.9\%$) and RUNX2+ cells ($18.4 \pm 0.8\%$) were decreased with miR-145 micelle treatment indicating that there were lower numbers of pathogenic, macrophage-like, and osteogenic cells in the plaques (Fig. 3D, F). The inhibitory effect of miR-145 micelles on VSMC dedifferentiation is further validated by the lower percentage of CD68 + YFP+ ($19.7 \pm 0.6\%$) and RUNX2+YFP + cells ($10.8 \pm 0.3\%$) in the plaque with miR-
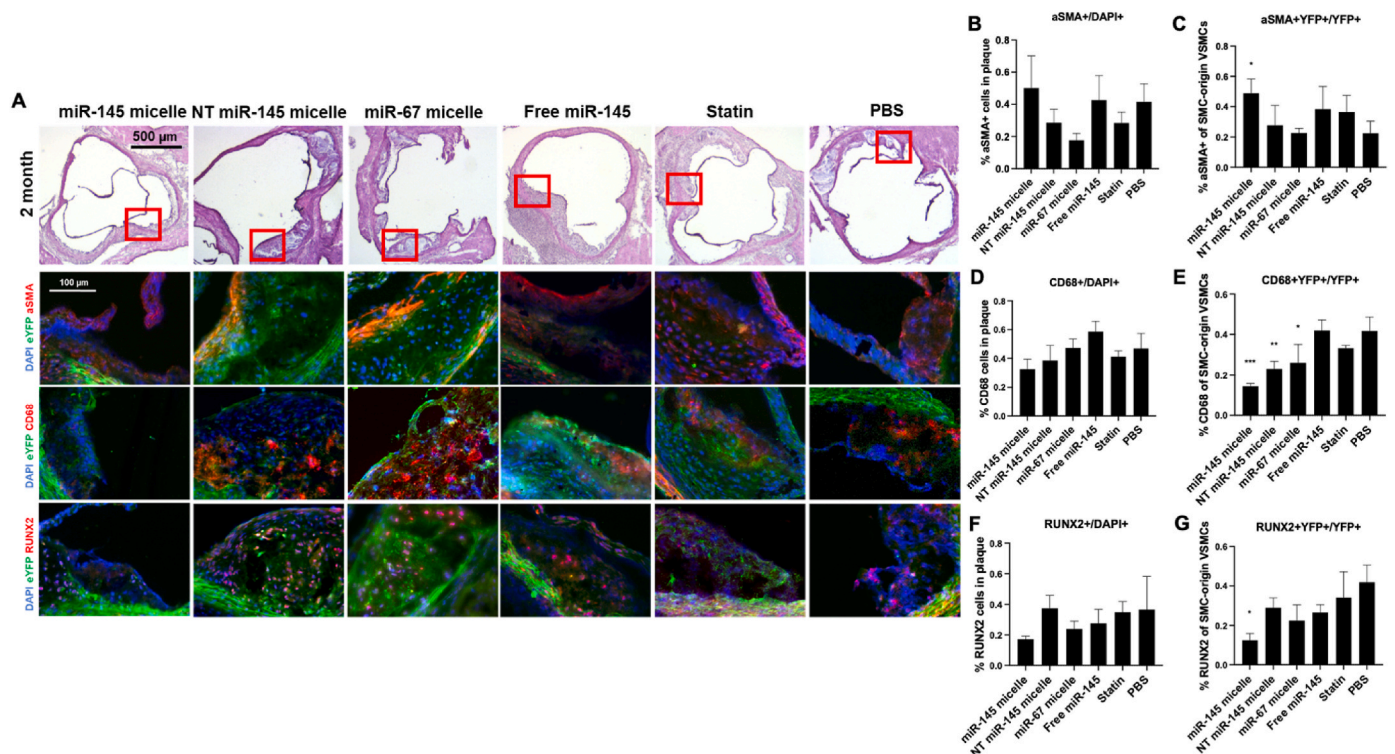
Fig. 6. Cellular composition of early-stage atherosclerotic plaque two months after treatment with a single dose of miR-145 micelles. (A) Immunohistochemistry of aortic root plaques for eYFP (green), α-SMA, CD68, RUNX2 (red), and nuclei (blue). Red boxes on H&E images indicate zoomed in areas of the aortic root (bottom). Quantification of cells expressing (B) α-SMA+/DAPI, (C) α-SMA + YFP+/YFP+, (D) CD68+/DAPI, (E) CD68 + YFP+/YFP+, (F) RUNX2+/DAPI, and (G) RUNX2+YFP+/YFP+. * indicates p < 0.05, **p < 0.01, ***p < 0.001.

145 micelle treatment compared to controls (PBS: 46.6 ± 9.8% and 31.3 ± 4%, respectively, Fig. 3E, G). Collectively, miR-145 micelles increase contractile SMC phenotype in plaques and reduce the overall presence of VSMC-derived macrophage-like and osteogenic cells at one month post single IV injection. The significant inhibition of plaque growth as seen in the smaller lesion sizes of miR-145 micelle-treated mice as well as the elevated miR-145 expression at the one-month time point suggest miR-145 micelles have a longer duration of action than the nanoparticle bioavailability in circulation (0.3 h half-life [26]).

3.2. Single dose miR-145 micelle effects on atherosclerosis after two months

3.2.1. Therapeutic evaluation after two months

Encouraged by the results from the one-month time point, we investigated even longer, sustained effects of miR-145 micelles in mice and studied its effects at two months after a single dose treatment. In the context of atherosclerosis therapies, hyperlipidemia drugs such as atorvastatin, are prescribed as daily medications, or for the recently FDA approved siRNA drug, inclisiran, every 3–6 months [45,46]. As shown in Fig. 4, miR-145 micelle treatment resulted in smaller plaques and reduced lesion area in the aortic root as compared to other treatment groups even after two months post-administration of a single dose of miR-145 micelles (miR-145 micelle: 6.7 ± 4.8%, NT miR-145 micelle: 14.5 ± 5.6%, miR-67 micelle: 16.9 ± 0.7%, free miR-145: 10.8 ± 5.0%, statin: 10.7 ± 3.6%, PBS: 14.6 ± 4.5%, p < 0.05 compared to PBS, Fig. 4A and B), which was validated by en face ORO staining (miR-145 micelle: 6.0 ± 2.2%, NT miR-145 micelle: 7.3 ± 0.7%, miR-67 micelle: 9.6 ± 0.9%, free miR-145: 8.0 ± 2.0%, statin: 8.2 ± 1.3%, PBS: 10.2 ± 1.8%, p < 0.05 compared to PBS, Fig. 4D and 5). Importantly, no significant decreases in plaque area were observed for statin treatment compared to the PBS control, indicating greater efficacy of miR-145 micelle compared to the clinical standard. No distinct trends were

seen for the necrotic core area based on treatment groups, although the necrotic core areas were smaller at this later time point for all treatment compared to the 1 month (1-month: 32.1 ± 22.3% vs 2-months: 30.4 ± 13.3%). This may be because advanced plaques are characterized by necrotic cores consisting of fibrosis and calcification, which have been reported to condense plaques and result in smaller lipid area [47].

Notably, when miR-145 expression in the aortic root was analyzed, miR-145 micelle treatment maintained a 1.3-fold increase in miR-145 expression compared to PBS treatment even after 2 months post-treatment. Our previous studies show that 90% of micelle constructs are eliminated within 10 h to 7 days [26,36]. Other miRs, such as miR-208 in rat hearts, have been shown to persist for weeks despite cessation of miR production, and in other cases, transfected miRs within fibroblasts show half-lives exceeding 100 h [48–51]. Thus, these studies demonstrate that miR stability or its effects may be longer lasting beyond its persistence in circulation [48]. Although it is unlikely that miR-145 micelles remain in circulation, it is possible that miR-145 micelles are retained within VSMCs due to their plaque-targeting capabilities [26], and thus, the extended therapeutic effect of miR-145 micelles may be due to the continued presence of miR-145 within cells and the long-lasting maintenance of contractile, healthy VSMC phenotype [26,36].

Additionally, endothelial cells and contractile VSMCs have been reported to release miR-145-containing exosomes that can reinforce the upregulation of miR-145 [52]. Thus, treatment of atherosclerosis with miR-145 micelles may help sustain vascular homeostasis resulting in healthy endothelial cells which in turn promote contractile VSMC phenotype via miR-145 exosome signaling [53,54].Overall, miR-145 micelles show prolonged effects in significantly inhibiting atherosclerosis progression which highlights their potential as a preventative treatment for atherosclerosis and will warrant future investigations into studying potential feedback mechanisms and cellular crosstalk within the vascular wall that may contribute to their sustained therapeutic
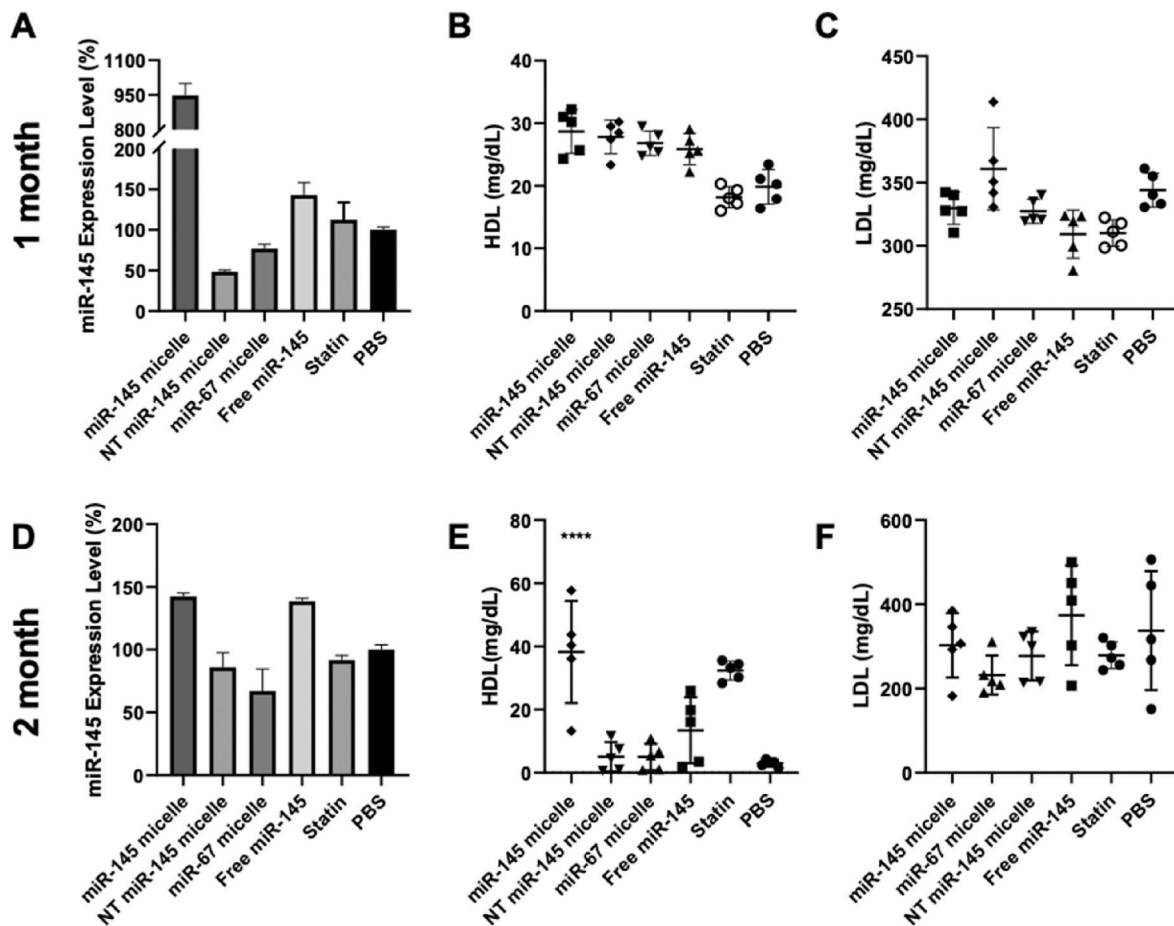
Fig. 7. Liver and cholesterol effects of miR-145 micelles. (A, D) miR-145 expression in the liver tissue determined via RT-qPCR for one month and two months post treatment. Serum (B, E) HDL and (C, F) LDL levels in treated mice. * indicates p < 0.05, **p < 0.01, ***p < 0.001, ****p < 0.0001.

effects [17,25,53].

3.2.2. Cellular composition of atherosclerotic plaques after two months

Similar to the one-month post treatment evaluation, cellular composition analyses were conducted to measure the effect of miR-145 micelles in VSMC phenotypic modulation two months after treatment. The overall trends at the two-month time point were similar to the one-month time point: miR-145 micelle treatment showed a larger proportion of α-SMA + cells (miR-145 micelles: 50.0 ± 20.1% vs PBS: 41.5 ± 11.3% vs statins: 20.6 ± 6.8%) and smaller proportion of CD68+ (miR-145 micelles: 32.6 ± 6.9% vs PBS: 46.8 ± 10.5% vs statins: 40.1 ± 4.1%) and RUNX2+ cells (miR-145 micelles: 17.1 ± 2.1% vs PBS: 36.6 ± 21.5% vs statins: 34.8 ± 7.0%) in plaques compared to PBS control, although not statistically significant (Fig. 6A). However, there were notable differences in the ratio of transformed VSMCs within plaques cells. The miR-145 micelle treatment showed the highest ratio of α-SMA + YFP + cells (48.8 ± 0.9%), lowest ratio of CD68 + YFP+ (14.5 ± 1.4%) and RUNX2+YFP + cells (12.5 ± 3.4%) compared to other treatment controls and PBS (22.5 ± 7.8%, p < 0.05; 41.7 ± 6.9%, p < 0.001; and 36.8 ± 12.0%, p < 0.05, respectively). Thus, miR-145 micelles continue to maintain the contractile VSMC phenotype, while inhibiting transdifferentiation of VSMCs into inflammatory macrophages or calcium-producing osteochondrogenic cells.

At both timepoints, the overall percentage of α-SMA + cells did not change within the plaque and α-SMA + YFP + cells remained high and unchanged with miR-145 micelle treatment. Similarly, the ratio of RUNX2+ cells and RUNX2+YFP + cells were lowest with miR-145 micelle treatment. Notably, the percentage of CD68 + YFP + decreased with miR-145 micelle treatment compared at two months,

despite an increase in the percentage of overall inflammatory CD68+ cells in the plaque. Based on these findings, we hypothesize that the early treatment with miR-145 micelles inhibits VSMC dedifferentiation and as a result, leads to sustained, downstream therapeutic consequences by minimizing VSMC transformation, migration, and proliferation, and thereby, resulting in limiting lesion growth [18]. As such, the results strongly support the viability of miR-145 micelles in mitigating atherosclerosis with dose intervals that are practical for atherosclerosis patients.

3.3. Effects of miR-145 micelles on liver and cholesterol

miR-145 micelles are primarily eliminated through the liver [26,55], similar to the majority of nanoparticles and drug delivery systems that have been developed. Thus, to analyze possible off-target effects, we analyzed miR-145 expression in the liver after treatment. As expected, miR-145 expression levels were higher in the liver upon miR-145 micelle treatment at both one month (9.5-fold increase compared to PBS) and two months (1.4-fold increase compared to PBS) post treatment (Fig. 7A, D). At the one-month timepoint, a 1.5-fold increase in liver miR-145 was also observed with free miR-145 treatment. However, histological analyses of the liver and other peripheral organ tissues with H&E stains show no significant differences in tissue morphology between different treatment groups (Figs. 8 and 9) and previous studies show no elevation in inflammatory cytokines [26]. This suggests that there are minimal toxic off-target effects that lead to damaging of peripheral organs rising from miR-145 micelle treatment.

Additionally, we analyzed the effects of miR-145 on cholesterol production and the reverse cholesterol transport system as an alternative
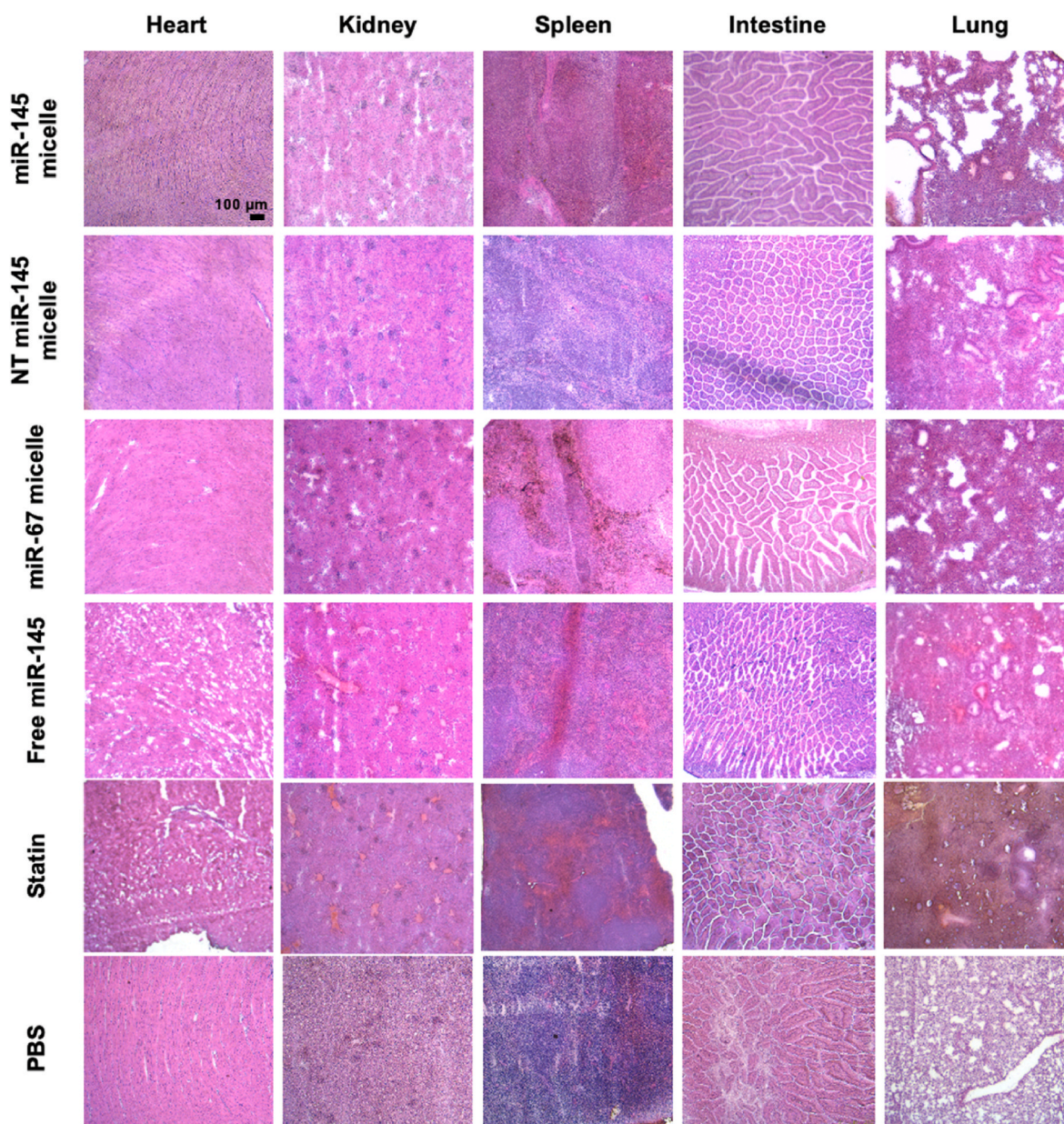
Fig. 8. H&E staining of peripheral organ sections at the one-month timepoint.

mechanism for lipid and necrotic core reduction in plaques, given miR-145 micelles are cleared in the liver. While there were no significant differences in serum HDL and LDL levels at one month post injection, miR-145 micelle treatment showed a significant upregulation of HDL at two months comparable to that of the statin treatment group (Fig. 7). HDL is involved in the reverse cholesterol transport system and is responsible for removing excess cholesterol from tissues and vessel walls through the liver, and it is possible that miR-145 is increasing macrophage cholesterol efflux of HDL [56,57], thus, providing an additional anti-atherogenic benefit [58–62]. However, additional studies are needed to determine the effects of miR-145 micelles on HDL biogenesis, function, circulation, and catabolism.

4. Conclusions

In summary, miR-145 micelles show anti-atherogenic effects lasting up to two months post single dose treatment, without causing toxicity. Specifically, miR-145 micelles maintained the healthy VSMC phenotype

and inhibited transition of VSMCs into alternative pathogenic cells such as macrophage-like and osteogenic cells. Furthermore, we show that miR-145 micelles can target the liver and play a role in reverse cholesterol transport through the elevation of HDL. As such, we demonstrate that miR-145 micelles have strong potential as a therapy for atherosclerosis, are more efficacious than the clinical standard statin treatment, and can be practically implemented with long dosing intervals for patients with chronic disease.

Ethics approval

The study protocol was reviewed and approved by the Institutional Animal Care and Use Committee (IACUC) at the University of Southern California.

CRediT authorship contribution statement

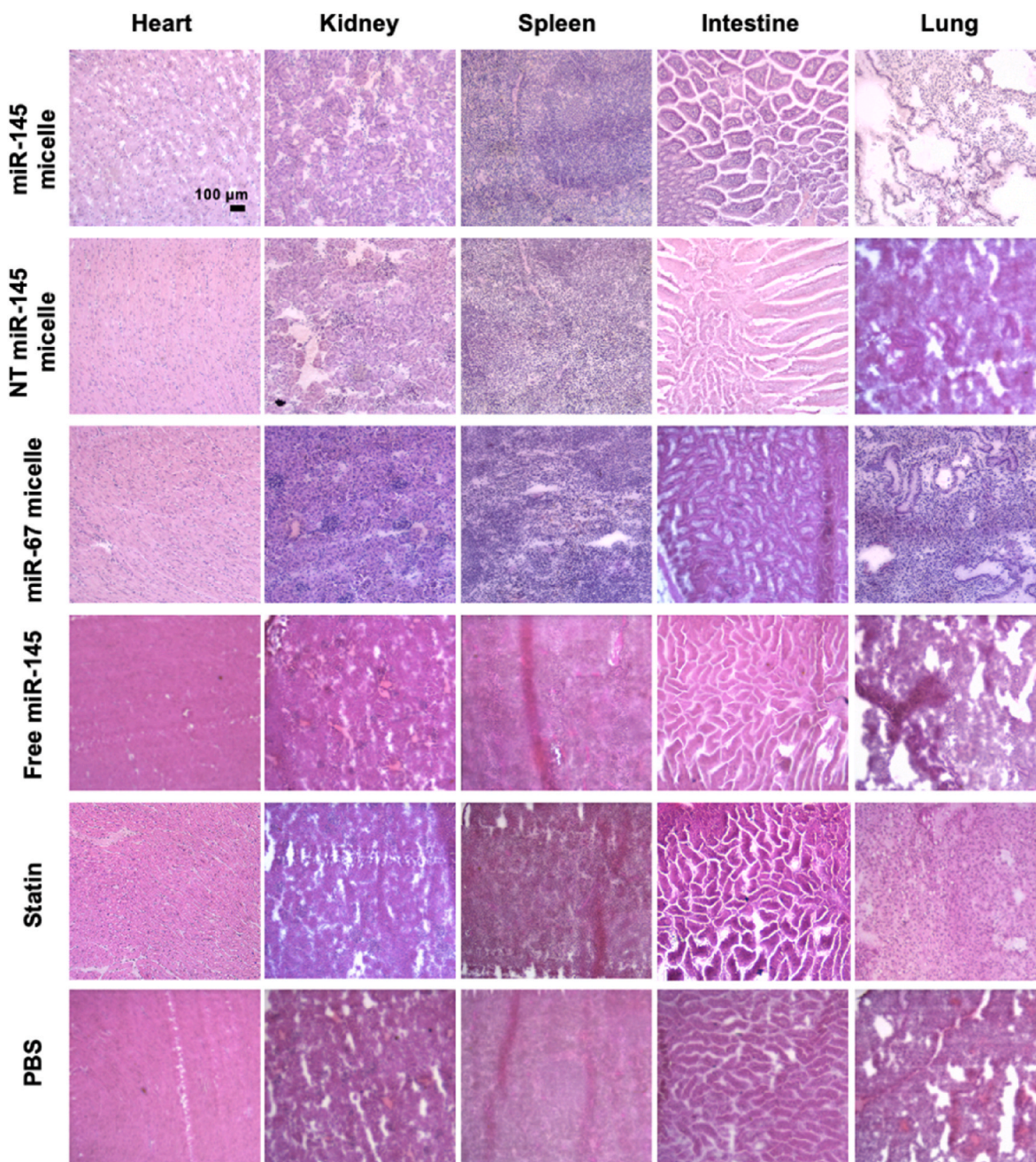**Deborah D. Chin:** conceived the project and designed the

Fig. 9. H&E staining of peripheral organ sections at the two-months timepoint.

experiments, performed the experiments and analyzed the data, and wrote the manuscript. **Neil Patel:** performed the experiments and analyzed the data, and wrote the manuscript. **Woori Lee:** performed the experiments and analyzed the data. **Sonali Kanaya:** performed the experiments and analyzed the data. **Jackson Cook:** performed the experiments and analyzed the data. **Eun Ji Chung:** conceived the project, designed the experiments, analyzed the data, wrote the manuscript, and obtained funding for the project, All authors have read and approved the final manuscript.

Declaration of competing interest

The authors declare that they have no known competing financial interests or personal relationships that could have appeared to influence the work reported in this paper.

Acknowledgements

Appendix A. Supplementary data

Supplementary data to this article can be found online at https://doi. org/10.1016/j.bioactmat.2023.04.001.

References

[1] T. Hoshino, et al., Mechanical stress analysis of a rigid inclusion in distensible material: a model of atherosclerotic calcification and plaque vulnerability, Am. J. Physiol. Heart Circ. Physiol. 297 (2) (2009) H802–H810.

[2] P.K. Shah, Mechanisms of plaque vulnerability and rupture, J. Am. Coll. Cardiol. 41 (4 Suppl S) (2003) 15S–22S.

[3] M. Ridker Paul, The JUPITER trial, Circ. Cardiovasc. Qual. Outcome. 2 (3) (2009) 279–285.

[4] P.M. Ridker, et al., Rosuvastatin to prevent vascular events in men and women with elevated C-reactive protein, N. Engl. J. Med. 359 (21) (2008) 2195–2207.

[5] H.V. Ganga, H.B. Slim, P.D. Thompson, A systematic review of statin-induced muscle problems in clinical trials, Am. Heart J. 168 (1) (2014) 6–15.

[6] N. Sattar, et al., Statins and risk of incident diabetes: a collaborative meta-analysis of randomised statin trials, Lancet 375 (9716) (2010) 735–742.

[7] I. Pinal-Fernandez, M. Casal-Dominguez, A.L. Mammen, Statins: pros and cons, Med. Clin. 150 (10) (2018) 398–402.

[8] C.K. Bradley, et al., Patient-reported reasons for declining or discontinuing statin therapy: insights from the PALM registry, J. Am. Heart Assoc. 8 (7) (2019) e011765.

[9] W. Herrington, et al., Epidemiology of atherosclerosis and the potential to reduce the global burden of atherothrombotic disease, Circ. Res. 118 (4) (2016) 535–546.

[10] Efficacy and safety of cholesterol-lowering treatment: prospective meta-analysis of data from 90 056 participants in 14 randomised trials of statins, Lancet 366 (9493) (2005) 1267–1278.

[11] P.P. Toth, et al., Management of statin intolerance in 2018: still more questions than answers, Am. J. Cardiovasc. Drugs : Drugs Dev. Other Interv. 18 (3) (2018) 157–173.

[12] S. Krähenbühl, I. Pavik-Mezzour, A. von Eckardstein, Unmet Needs in LDL-C Lowering: When Statins Won't Do! Drugs 76 (12) (2016) 1175–1190.

[13] A. Pradhan, M. Bhandari, R. Sethi, Ezetimibe and improving cardiovascular outcomes: current evidence and perspectives, Cardiol. Res. Pract. 2020 (2020) 9815016, 9815016.

[14] M.O.J. Grootaert, M.R. Bennett, Vascular smooth muscle cells in atherosclerosis: time for a re-assessment, Cardiovasc. Res. 117 (11) (2021) 2326–2339.

[15] V.P. Iyemere, et al., Vascular smooth muscle cell phenotypic plasticity and the regulation of vascular calcification, J. Intern. Med. 260 (3) (2006) 192–210.

[16] J. Chappell, et al., Extensive proliferation of a subset of differentiated, yet plastic, medial vascular smooth muscle cells contributes to neointimal formation in mouse injury and atherosclerosis models, Circ. Res. 119 (12) (2016) 1313–1323.

[17] S. Feil, et al., Transdifferentiation of vascular smooth muscle cells to macrophage-like cells during atherogenesis, Circ. Res. 115 (7) (2014) 662–667.

[18] K. Jacobsen, et al., Diverse cellular architecture of atherosclerotic plaque derives from clonal expansion of a few medial SMCs, JCI Insight 2 (19) (2017).

[19] M.Y. Speer, et al., Smooth muscle cells give rise to osteochondrogenic precursors and chondrocytes in calcifying arteries, Circ. Res. 104 (6) (2009) 733–741.

[20] N. Patel, D.D. Chin, E.J. Chung, Exosomes in atherosclerosis, a double-edged sword: their role in disease pathogenesis and their potential as novel therapeutics, AAPS J. 23 (5) (2021) 95.

[21] J.F. Bentzon, et al., Mechanisms of plaque formation and rupture, Circ. Res. 114 (12) (2014) 1852–1866.

[22] Y.V. Bobryshev, et al., Matrix vesicles in the fibrous cap of atherosclerotic plaque: possible contribution to plaque rupture, J. Cell Mol. Med. 12 (5B) (2008) 2073–2082.

[23] M. Naghavi, et al., From vulnerable plaque to vulnerable patient: a call for new definitions and risk assessment strategies: Part II, Circulation 108 (15) (2003) 1772–1778.

[24] A.N. Kapustin, et al., Vascular smooth muscle cell calcification is mediated by regulated exosome secretion, Circ. Res. 116 (8) (2015) 1312–1323.

[25] G.F. Alencar, et al., Stem cell pluripotency genes Klf4 and Oct 4 regulate complex SMC phenotypic changes critical in late-stage atherosclerotic lesion pathogenesis, Circulation 142 (21) (2020) 2045–2059.

[26] D.D. Chin, et al., miR-145 micelles mitigate atherosclerosis by modulating vascular smooth muscle cell phenotype, Biomaterials 273 (2021), 120810.

[27] N. Patel, et al., Therapeutic response of miR-145 micelles on patient-derived vascular smooth muscle cells, Front. Digit. Health 4 (2022), 836579.

[28] L.S. Shankman, et al., KLF4-dependent phenotypic modulation of smooth muscle cells has a key role in atherosclerotic plaque pathogenesis, Nat. Med. 21 (6) (2015) 628–637.

[29] A.Y. Rangrez, et al., miR-143 and miR-145, Circ. Cardiovasc. Genet. 4 (2) (2011) 197–205.

[30] E.J. Chung, et al., Monocyte-targeting supramolecular micellar assemblies: a molecular diagnostic tool for atherosclerosis, Adv. Healthc. Mater. 4 (3) (2015) 367–376.

[31] G. Spinetti, et al., Rat aortic MCP-1 and its receptor CCR2 increase with age and alter vascular smooth muscle cell function, Arterioscler. Thromb. Vasc. Biol. 24 (8) (2004) 1397–1402.

[32] H. Zogg, R. Singh, S. Ro, Current advances in RNA therapeutics for human diseases, Int. J. Mol. Sci. 23 (5) (2022).

[33] M.A. Alfaleh, et al., Targeting mesothelin receptors with drug-loaded bacterial nanocells suppresses human mesothelioma tumour growth in mouse xenograft models, PLoS One 12 (10) (2017) e0186137.

[34] S.M. Hoy, Patisiran: first global approval, Drugs 78 (15) (2018) 1625–1631.

[35] D.D. Chin, et al., Hydroxyapatite-binding micelles for the detection of vascular calcification in atherosclerosis, J. Mater. Chem. B 7 (41) (2019) 6449–6457.

[36] E.J. Chung, et al., Fibrin-binding, peptide amphiphile micelles for targeting glioblastoma, Biomaterials 35 (4) (2014) 1249–1256.

[37] E.J. Chung, et al., In vivo biodistribution and clearance of peptide amphiphile micelles, Nanomedicine 11 (2) (2015) 479–487.

[38] A. Chattopadhyay, et al., Cholesterol-Induced phenotypic modulation of smooth muscle cells to macrophage/fibroblast–like cells is driven by an unfolded protein response, Arterioscler. Thromb. Vasc. Biol. 41 (1) (2021) 302–316.

[39] J.J. Patel, et al., Inhibition of arterial medial calcification and bone mineralization by extracellular nucleotides: the same functional effect mediated by different cellular mechanisms, J. Cell. Physiol. 233 (4) (2018) 3230–3243.

[40] D. Adams, et al., Long-term safety and efficacy of patisiran for hereditary transthyretin-mediated amyloidosis with polyneuropathy: 12-month results of an open-label extension study, Lancet Neurol. 20 (1) (2021) 49–59.

[41] D. Adams, et al., Patisiran, an RNAi therapeutic, for hereditary transthyretin amyloidosis, N. Engl. J. Med. 379 (1) (2018) 11–21.

[42] G.L. Basatemur, et al., Vascular smooth muscle cells in atherosclerosis, Nat. Rev. Cardiol. 16 (12) (2019) 727–744.

[43] A.L. Durham, et al., Role of smooth muscle cells in vascular calcification: implications in atherosclerosis and arterial stiffness, Cardiovasc. Res. 114 (4) (2018) 590–600.

[44] A. Daugherty, et al., Recommendation on design, execution, and reporting of animal atherosclerosis studies: a scientific statement from the American heart association, Arterioscler. Thromb. Vasc. Biol. 37 (9) (2017) e131–e157.

[45] K.K. Ray, et al., Inclisiran in patients at high cardiovascular risk with elevated LDL cholesterol, N. Engl. J. Med. 376 (15) (2017) 1430–1440.

[46] D.K. Arnett, et al., 2019 ACC/AHA guideline on the primary prevention of cardiovascular disease: executive summary: a report of the American college of cardiology/American heart association task force on clinical practice guidelines, J. Am. Coll. Cardiol. 74 (10) (2019) 1376–1414.

[47] H.C. Stary, Natural history and histological classification of atherosclerotic lesions: an update, Arterioscler. Thromb. Vasc. Biol. 20 (5) (2000) 1177–1178.

[48] M.P. Gantier, et al., Analysis of microRNA turnover in mammalian cells following Dicer 1 ablation, Nucleic Acids Res. 39 (13) (2011) 5692–5703.

[49] E. van Rooij, et al., Control of stress-dependent cardiac growth and gene expression by a microRNA, Science 316 (5824) (2007) 575–579.

[50] S. Bail, et al., Differential regulation of microRNA stability, RNA 16 (5) (2010) 1032–1039.

[51] Y. Guo, et al., Characterization of the mammalian miRNA turnover landscape, Nucleic Acids Res. 43 (4) (2015) 2326–2341.

[52] A.Y. Rangrez, et al., miR-143 and miR-145: molecular keys to switch the phenotype of vascular smooth muscle cells, Circ. Cardiovasc. Genet. 4 (2) (2011) 197–205.

[53] N. Méndez-Barbero, C. Gutiérrez-Muñoz, L.M. Blanco-Colio, Cellular crosstalk between endothelial and smooth muscle cells in vascular wall remodeling, Int. J. Mol. Sci. 22 (14) (2021) 7284.

[54] E. Hergenreider, et al., Atheroprotective communication between endothelial cells and smooth muscle cells through miRNAs, Nat. Cell Biol. 14 (3) (2012) 249–256.

[55] C. Poon, et al., Protein Mimetic and Anticancer Properties of Monocyte-Targeting Peptide Amphiphile Micelles, ACS Biomaterials Science & Engineering, 2017.

[56] J.Y. Lee, J.S. Parks, ATP-binding cassette transporter AI and its role in HDL formation, Curr. Opin. Lipidol. 16 (1) (2005) 19–25.

[57] X. Zhou, et al., Inhibition of ERK1/2 and activation of liver X receptor synergistically induce macrophage ABCA1 expression and cholesterol efflux, J. Biol. Chem. 285 (9) (2010) 6316–6326.

[58] M. Barylski, et al., Emerging therapies for raising high-density lipoprotein cholesterol (HDL-C) and augmenting HDL particle functionality, Best Pract. Res. Clin. Endocrinol. Metabol. 28 (3) (2014) 453–461.

[59] M.H. Davidson, P.P. Toth, High-density lipoprotein metabolism: potential therapeutic targets, Am. J. Cardiol. 100 (11 A) (2007) n32–n40.

[60] M.B. Elshazly, et al., Patient-level discordance in population percentiles of the total cholesterol to high-density lipoprotein cholesterol ratio in comparison with low-density lipoprotein cholesterol and non-high-density lipoprotein cholesterol: the very large database of lipids study (VLDL-2B), Circulation 132 (8) (2015) 667–676.

[61] M. Kaur, et al., Effect of high-density lipoprotein cholesterol levels on overall survival and major adverse cardiovascular and cerebrovascular events, Am. J. Cardiol. 146 (2021) 8–14.

[62] P.P. Toth, High-density lipoprotein: epidemiology, metabolism, and antiatherogenic effects, Dis. Mon. 47 (8) (2001) 369–416.